

Synthesizing three-body interaction of spin chirality with superconducting qubits

Wuxin Liu,^{1, a)} Wei Feng,^{1, a)} Wenhui Ren,¹ Da-Wei Wang,^{1, b)} and H. Wang^{1, c)}

¹ *Interdisciplinary Center for Quantum Information and Zhejiang Province Key Laboratory of Quantum Technology and Device, Department of Physics, Zhejiang University, Hangzhou 310027, China*

(Dated: 7 February 2020)

Superconducting qubits provide a competitive platform for quantum simulation of complex dynamics that lies at the heart of quantum many-body systems, because of the flexibility and scalability afforded by the nature of microfabrication. However, in a multiqubit device, the physical form of couplings between qubits is either an electric (capacitor) or magnetic field (inductor), and the associated quadratic field energy determines that only two-body interaction in the Hamiltonian can be directly realized. Here we propose and experimentally synthesize the three-body spin-chirality interaction in a superconducting circuit based on Floquet engineering. By periodically modulating the resonant frequencies of the qubits connected with each other via capacitors, we can dynamically turn on and off qubit-qubit couplings, and further create chiral flows of the excitations in the three-qubit circular loop. Our result is a step toward engineering dynamical and many-body interactions in multiqubit superconducting devices, which potentially expands the degree of freedom in quantum simulation tasks.

Quantum simulation is an efficient way to solve the classically inaccessible many-body problems of complex quantum systems¹. Among different strategies, analog quantum simulation, which intuitively uses a controllable quantum system to mimic the Hamiltonian of a target one, is more attainable in the near future because of its higher tolerance level of errors^{2,3}. Superconducting qubits with advantages in flexibility and scalability are one of the leading candidates for building a practical analog quantum simulator⁴⁻⁷. In a multiqubit superconducting circuit, qubits are typically connected by capacitors/inductors which store electric/magnetic fields, and the coupling energy contribution to the Hamiltonian depends quadratically on the field operators. Therefore it is straightforward to implement the two-body flip-flop interaction in the isotropic spin-1/2 XY -type model through the capacitive or inductive coupling⁸. However, interactions containing more spin operators, which are useful in calculating the ground state energy of molecules^{9,10} and in toric codes¹¹, remain challenging to be experimentally realized.

Floquet engineering characterized by fast periodic modulation of the characteristic frequencies of a quantum system is a versatile way to control the long-time dynamics of the system¹². The key of Floquet engineering is designing appropriate driving schemes to synthesize the target Hamiltonian. In superconducting qubits, Floquet engineering has been used to realize chiral ground state current¹³, quantum switch¹⁴, perfect state transfer¹⁵, Dzyaloshinskii-Moriya (DM) interaction¹⁶, and topological magnon insulator states¹⁷. Although it has been proven in theory that arbitrary two-body spin inter-

actions can be synthesized by Floquet modulation^{18,19}, many exotic phenomena, such as topological phases with anyonic excitations²⁰, can only appear as a direct consequence of the many-body interactions involving more than two spins²¹.

Spin chirality²² represents one example of the many-body interactions involving three spins, $\hat{\chi} = \boldsymbol{\sigma}_1 \cdot (\boldsymbol{\sigma}_2 \times \boldsymbol{\sigma}_3)$, where $\boldsymbol{\sigma}_j = (\sigma_j^x, \sigma_j^y, \sigma_j^z)$ is the Pauli vector for the j th spin-1/2 particle. It plays an important role in quantum Hall effect in magnetic materials²³⁻²⁸ and chiral spin states in spin liquids^{29,30}. The dynamics driven by $\hat{\chi}$ features a chiral evolution of the three-spin states $|s_1 s_2 s_3\rangle$, i.e., $e^{-i\hat{\chi}\theta}|s_1 s_2 s_3\rangle = |s_3 s_1 s_2\rangle$, with $\theta = \pi/3\sqrt{3}$ and $s_j = 0$ (spin down) or 1 (spin up). It can be used in perfect state transfer³¹ for arbitrary three-spin states. By changing $\hat{\chi} \rightarrow -\hat{\chi}$, the rotation direction of the spin states is reversed. It is worth noting that $\hat{\chi}$ breaks both the time reversal symmetry T (replacing $\boldsymbol{\sigma}_j$ with $-\boldsymbol{\sigma}_j$) and parity symmetry P (exchanging $\boldsymbol{\sigma}_i \leftrightarrow \boldsymbol{\sigma}_j$) but conserves the PT symmetry²².

Here we propose and experimentally demonstrate a method to synthesize the three-body spin chirality interaction $\hat{\chi}$, based on Floquet engineering for three superconducting qubits that are pair-wisely connected. By periodically modulating the resonant frequencies of the three qubits with well-controlled amplitudes, periods, and phases, we can dynamically turn on and off the coupling between any two qubits, and further create the three-body term $\hat{\chi}$ in the effective Hamiltonian. Under the engineered $\hat{\chi}$, we characterize the three-qubit chiral dynamics where excitations injected to one or two of the qubits flow clockwise through the three-qubit sites, which is in excellent agreement with numerical simulation taking into account qubit anharmonicity. The capability of engineering dynamical and many-body interactions beyond the conventional two-body ones will certainly expand the functionality of the quantum simulation plat-

^{a)}W. L. and W. F. contributed equally to this work.

^{b)}Electronic mail: dwwang@zju.edu.cn

^{c)}Electronic mail: hhwang@zju.edu.cn

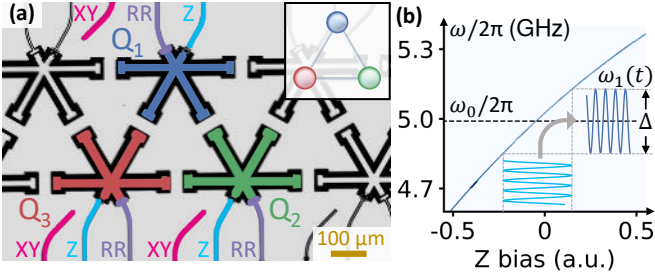


FIG. 1. (a) False color image of the three qubits, as labeled, for synthesizing the three-body interaction $\hat{\chi}$. Inset: Cartoon illustration of the three qubits arranged in a circular loop. (b) Resonant frequency as a function of Z line bias for Q_1 , which is used to calibrate the nearly-sinusoidal Z pulse (light blue sinusoid) for modulating the qubit frequency with the desired amplitude Δ (dark blue sinusoid).

form built upon multiqubit superconducting circuits.

The multiqubit superconducting device used in this experiment is illustrated in Fig. 1(a), where frequency-tunable transmon qubits^{32,33} are arranged in a triangular chain, and each qubit is capacitively coupled to four neighbors with the coupling strength $g/2\pi$ ranging from 10 to 13 MHz. To synthesize $\hat{\chi}$, we focus on the three qubits Q_1 , Q_2 , and Q_3 as highlighted by colors of blue, green, and red in Fig. 1(a), respectively, while all the other qubits (light gray) are far detuned in frequency. Assuming that the pair-wise coupling strengths are uniform, the three-qubit Hamiltonian is

$$H = \hbar \sum_{j=1}^3 \omega_j(t) \sigma_j^+ \sigma_j^- + \hbar g \sum_{jk} (\sigma_j^+ \sigma_k^- + \sigma_j^- \sigma_k^+), \quad (1)$$

where σ_j^+ and σ_j^- are Q_j 's raising and lowering operators, respectively. As labeled in Fig. 1, each qubit Q_j has a microwave drive line (magenta) to inject excitations for XY rotations, a flux line (cyan) to tune the resonant frequency $\omega_j(t)$ for Z rotations, and a readout resonator (purple) for detecting the state of the qubit. Single-qubit π rotations used in the experiment are calibrated to be around 0.997 in fidelity by randomized benchmarking. Detailed device parameters such as qubit coherence times, readout fidelities, and qubit-qubit coupling strengths can be found in Supplementary Material.

As illustrated in Fig. 1(b), with Floquet engineering, we apply periodic driving signals through the Z line of Q_j , so that Q_j 's resonant frequency varies over time according to $\omega_j(t) = \omega_j(0) + \Delta_j \cos(\nu_j t + \phi_j)$, where values of $\omega_j(0)$, Δ_j , ν_j , and ϕ_j are properly chosen depending on the function to be achieved ($\Delta_j, \nu_j \gg g$). The Floquet driving signals can be applied to one, two, or all three qubits simultaneously, and for simplicity here we assume $\omega_j(0) \equiv \omega_0$, $\Delta_j \equiv \Delta$, and $\nu_j \equiv \nu$ for all qubits being modulated. For example, in the interaction picture, Eq. (1) becomes

$$H_I = \hbar g \sigma_j^+ \sigma_k^- e^{i(\Delta/\nu)[\sin(\nu t + \phi_j) - \sin(\nu t + \phi_k)]} + \text{h.c.}, \quad (2)$$

if both Q_j and Q_k are being modulated while the third qubit is far detuned and can be ignored. Using the Jacobi-Anger expansion $e^{iz \sin(y)} = \sum_{n=-\infty}^{+\infty} J_n(z) e^{iny}$, where $J_n(z)$ is the n th-order Bessel function of the first kind, the interaction Hamiltonian can be expanded to

$$H_I = \sum_{n=-\infty}^{+\infty} H_n e^{in\nu t}, \quad (3)$$

where H_n contains the two-body operators $\sigma_j^+ \sigma_k^-$.

For two qubits, a direct consequence of Eq. (3) is that the time-independent zeroth-order term in H_I dominates the long-time dynamics ($\gg 2\pi/\nu$) while the net contribution of all higher order terms ($|n| \geq 1$) is zero. The zeroth-order term determines that the effective coupling strength, g_{eff} , between Q_j and Q_k under the Floquet engineering is $gJ_0(2 \sin(\delta\phi/2)\Delta/\nu)$, which can be tuned by varying the ratio of Δ/ν and the relative phase between the two Floquet driving signals $\delta\phi = \phi_j - \phi_k$. An experiment is done to verify such a tunability based on the pulse sequence illustrated in Fig. 2(a), in which Rabi oscillations between Q_1 and Q_2 are mapped out at different $\delta\phi$ values with $\omega_0/2\pi \approx 4.990$ GHz, $\nu/2\pi = 100$ MHz, and

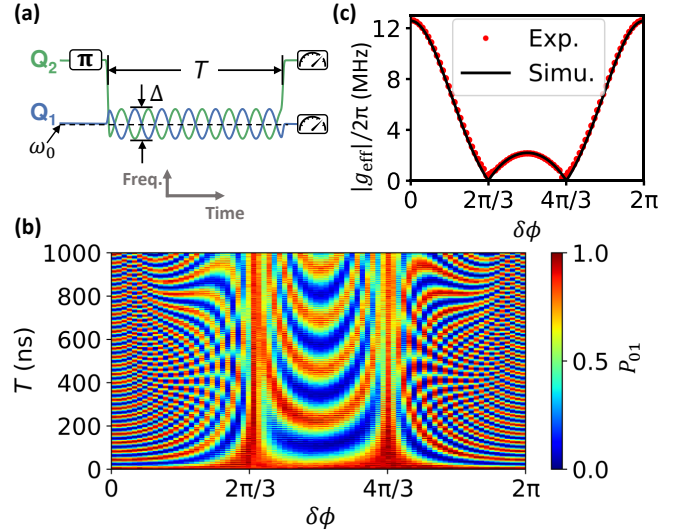


FIG. 2. (a) Pulse sequence to tune the effective coupling strength g_{eff} between Q_1 and Q_2 by applying Floquet driving signals to the two qubits simultaneously. The sequence starts with initializing both Q_1 and Q_2 in $|0\rangle$ (Q_3 is far detuned), and then exciting Q_2 to $|1\rangle$ with a π rotation, following which both qubits are modulated via sinusoidal signals centering around 4.990 GHz through their Z lines for a period of T . The two sinusoidal signals have the same amplitude Δ and frequency ν , but differ in phase by $\delta\phi$. Finally the two-qubit joint state is measured after the Floquet modulation. (b) Experimental probability of the Q_1 - Q_2 joint state $|01\rangle$ as a function of T and $\delta\phi$. At fixed $\delta\phi$ along the time axis, Rabi oscillations with varying periods are clearly observed. (c) Effective coupling strength $|g_{\text{eff}}|$ obtained by Fourier transform of the data in (b) as a function of $\delta\phi$ (dots), in comparison with the numerical simulation result (line).

$\Delta/2\pi \approx 138$ MHz. At $\delta\phi = 2\pi/3$ or $4\pi/3$, the oscillation patterns disappear as $g_{\text{eff}} = 0$, which indicates that the two qubits are dynamically decoupled. In Fig. 2(c), $|g_{\text{eff}}|$ as a function of $\delta\phi$ (dots) is obtained by Fourier transform of the data in Fig. 2(b) along the time axis, which is in excellent agreement with the numerical simulation result (line). We note that the tunability of g_{eff} can also be realized by modulating just one of the two qubits. However, the modulation amplitude Δ has to be about twice larger in order to completely decouple the two qubits, which is experimentally more difficult and may further expose the qubit to the impact of two-level state defects in the spectrum (see Supplementary Material).

Now we show that by applying periodic driving signals through the Z lines to all three qubits simultaneously, so that Q_j 's resonant frequency is modulated according to $\omega_j(t) = \omega_0 + \Delta \cos(\nu t + 2\pi j/3)$, it is possible to observe the long-time dynamics governed by the three-body $\hat{\chi}$ interaction. The strategy is the same as before: Take the summation over all pair-wise terms similar to that in Eq. (2) and follow the Jacobi-Anger expansion to obtain Eq. (3) for the three-qubit case, where $H_n = \hbar g i^n J_n (\sqrt{3}\Delta/\nu) e^{in(j+k)\pi/3} \sum_{jk} [\sigma_j^+ \sigma_k^- + (-1)^n \sigma_j^- \sigma_k^+]$. Note that H_n is the Hermitian conjugate of H_{-n} . At $\nu \gg g$, the second order perturbation is valid, and the effective Hamiltonian governing the long-time dynamics is^{12,34}

$$H_{\text{eff}} \approx H_0 + \sum_{n=1}^{\infty} \frac{1}{n\hbar\nu} [H_n, H_{-n}], \quad (4)$$

where $[H_n, H_{-n}] \propto \sum_{jkl} \sigma_j^z (\sigma_k^x \sigma_l^y - \sigma_k^y \sigma_l^x)$. Finally, with the chirality operator $\hat{\chi}$, we rewrite

$$H_{\text{eff}} = H_0 + \hbar\kappa\hat{\chi}, \quad (5)$$

where $\kappa = g^2\beta/\nu$ and $\beta = \sum_{n=1}^{\infty} J_n^2 (\sqrt{3}\Delta/\nu) \sin(n\pi/3)/n$ (see Supplementary Material).

Under the engineered $\hat{\chi}$, excitations injected to one or two of the qubits will flow clockwise through the three-qubit sites (see Supplementary Material for the tune-up procedure). Figure 3 shows such an experiment where a single excitation injected to one of the qubits travels cyclically through the three-qubit sites under the Floquet modulation. The modulation parameters are chosen $\omega_0/2\pi \approx 4.990$ GHz, $\Delta/2\pi \approx 138$ MHz, $\nu/2\pi = 100$ MHz for all three qubits, and $\delta\phi \approx 2\pi/3$ between any pair of qubits, which result in zero effective coupling strength for any pair of qubits, i.e., $H_0 = 0$ in Eq. (5), as confirmed in Fig. 2. With the pulse sequence in Fig. 3(a), we initialize $|Q_1 Q_2 Q_3\rangle$ in $|001\rangle$ with a π rotation to Q_3 , then apply the Floquet modulation signals through qubit Z lines for a period of T , and finally tune all qubits quickly to their idle frequencies for simultaneous readout. As shown in Figs. 3(b) and (c), the measured probabilities of the three single-excitation multiqubit states $|001\rangle$, $|010\rangle$, and $|100\rangle$ as functions of T are plotted in Fig. 3(b), which indicates that the excitation circulates along the route

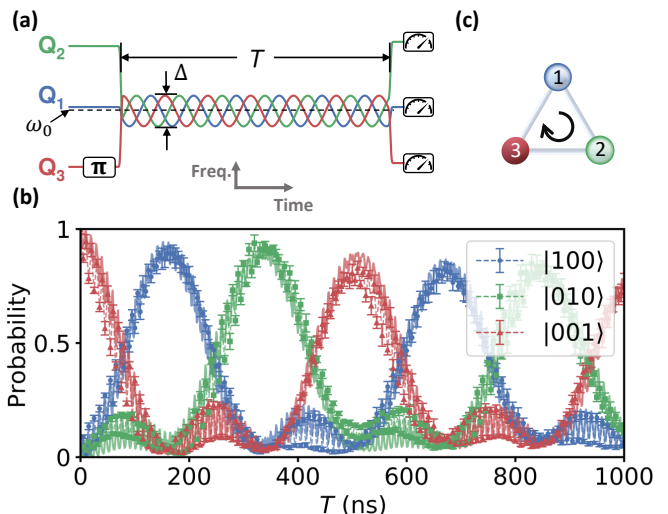


FIG. 3. (a) Pulse sequence for observing the single-excitation chiral dynamics. (b) Measured probabilities of the single-excitation multiqubit states (symbols connected by dashed lines) as functions of the modulation time T . Data curves of P_{100} , P_{010} , and P_{001} , colored according to the site colors containing the excitation in (c), rise up sequentially and cyclically, indicating the chiral motion of the single excitation. Error bars are standard deviations of five repetitive measurements. Solid lines are the numerical simulation results. (c) Schematics of the chiral dynamics, where the dark (light) color represents the qubit in $|1\rangle$ ($|0\rangle$) and the arrow indicates the rotation direction of the single excitation.

$Q_3 \rightarrow Q_1 \rightarrow Q_2 \rightarrow Q_3$. The numerical simulation results taking into account realistic device and experimental parameters are also plotted for comparison. In the numerical simulation, the control parameters Δ_j , $\delta\phi_j$, and $\delta\omega_{0,j}$ in Q_j 's Floquet drive $\omega_j(t) = (\bar{\omega}_0 + \delta\omega_{0,j}) + \Delta_j \cos(\nu t + \delta\phi_j)$ are set as $\Delta_j/2\pi = \{138 \text{ MHz}, 140 \text{ MHz}, 136 \text{ MHz}\}$, $\delta\phi_j = \{-0.1, 2\pi/3, 4\pi/3 + 0.1\}$, and $\delta\omega_{0,j}/2\pi = \{0, 0.7 \text{ MHz}, 0\}$ for $Q_j = \{Q_1, Q_2, Q_3\}$. The choice of these parameter values yields a good numerical match with the experimental data, which is also reasonable considering how we tune up the experiment.

For bosons with on-site repulsive interactions in a synthetic gauge field or spins with DM interactions, the chiral evolution of a double-excitation state, equivalent to the presence of a vacancy in the three-qubit sites, is opposite to that of a single-excitation state. However, with the spin chirality interaction, directions of the chiral evolutions of these two states are the same. To verify this point, here we initialize the three-qubit state in $|011\rangle$ to obtain the double-excitation chiral dynamics using the pulse sequence shown in Fig. 4(a). We observe that the double excitations collectively circulate clockwise, i.e., the vacancy in excitations (the $|0\rangle$ state) circulates along the route $Q_1 \rightarrow Q_2 \rightarrow Q_3 \rightarrow Q_1$ as shown in Figs. 4(b) and (c), in the same direction as that for the single-excitation state in Figs. 3(b) and (c). However, we notice non-negligible decreases of the modulation am-

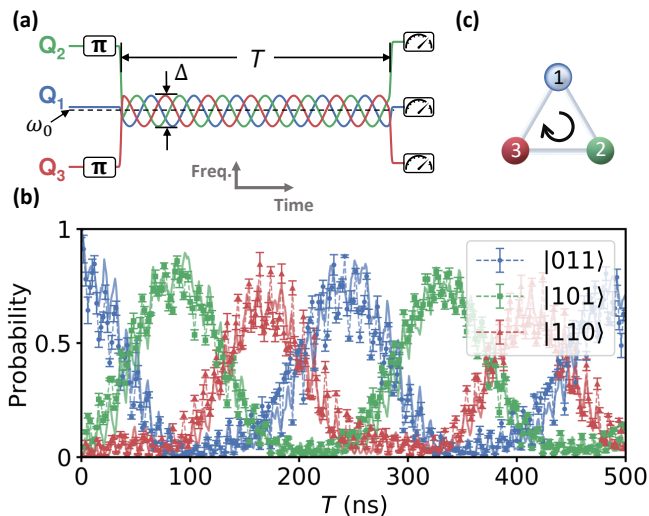


FIG. 4. (a) Pulse sequence for observing the double-excitation chiral dynamics. (b) Measured probabilities of the double-excitation multiqubit states (symbols connected by dashed lines) as functions of the modulation time T . Data curves of P_{011} , P_{101} , and P_{110} , colored according to the colors of the vacancy sites in (c), rise up sequentially and cyclically, indicating the chiral motion of the vacancy (or the double excitations). Error bars are standard deviations of five repetitive measurements. Solid lines are the numerical simulation results. (c) Schematics of the chiral dynamics, where the dark (light) color represents the qubit in $|1\rangle$ ($|0\rangle$) and the arrow indicates the rotation direction of the vacancy (or the double excitations).

plitudes for all three qubits (here $\Delta/2\pi \approx 135$ MHz), and meanwhile we observe that the time for completing a full cycle is almost one-half of the time for the single-excitation cycle. These are due to the existence of the third energy level $|2\rangle$ in the transmon qubits, where the qubit anharmonicity $\eta/2\pi$, i.e., the frequency difference between the $|1\rangle \leftrightarrow |2\rangle$ and $|0\rangle \leftrightarrow |1\rangle$ transitions, is about -230 MHz. When there are two excitations, e.g., $|011\rangle$ for $|Q_1 Q_2 Q_3\rangle$, an additional coupling channel between Q_1 in $|0\rangle$ and Q_3 in $|1\rangle$ exists via the second-order effect mediated by Q_2 's $|1\rangle \leftrightarrow |2\rangle$, and the same is between Q_1 and Q_2 . As confirmed by the analysis in Supplementary Material and the numerical simulation results taking into account the qubit anharmonicity in Figs. 4(b), the additional second-order effective interaction mediated by $|2\rangle$ indeed reduces the modulation amplitudes and accelerates the circulation as expected (see Supplementary Material).

In our experiment, the three-body chirality interaction is a second-order effect under the approximation $\nu \gg g$, and the resulting interaction strength is estimated to be $\kappa/2\pi \approx 0.5$ MHz, which is sufficient for the observation of the chiral dynamics. Although this interaction strength is relatively weak and the second-order effect may not allow the implementation of high-fidelity quantum gates, our method of synthesizing the three-body interaction can still be useful for analog quantum simulation, since it

is generally difficult to create a dynamical process mimicking that under a many-body Hamiltonian using the experimentally available one- and two-qubit gates (see, e.g., the recent experiment of generating multicomponent atomic Schrödinger cat states of up to 20 superconducting qubits³³).

In summary, we experimentally demonstrate a method for synthesizing three-body interaction of spin chirality with three superconducting qubits arranged in a triangular loop. This method expands the interaction types that we can achieve in superconducting qubits. Meanwhile, the models that contain three-body interaction for qubits arranged in triangular lattices were shown to have multi-degenerate ground states^{35–38}. The degeneracy depends on the topology of the system and is well protected against perturbations. Our experiment provides one possible way to realize these models and the ground states of these Hamiltonian can be used in the implementation of topological physics.

Supplementary Material

See Supplementary Material for device parameters, the experiment of tuning the qubit-qubit coupling by Floquet modulation of just one qubit, the tune-up procedure of the three-qubit Floquet modulations for the chiral dynamics, and the detailed theoretical analysis of the interaction Hamiltonian for both the single- and double-excitation cases.

Acknowledgments

We thank Hekang Li and Dongning Zheng for fabricating the device, and Chao Song, Qiujiang Guo, and Zhen Wang for technical support during the experiment. This work was supported by the National Key Research and Development Program of China (Grants No. 2019YFA0308100) and the National Natural Science Foundations of China (Grants No. 11725419 and No. 11874322).

- ¹R. P. Feynman, “Simulating physics with computers,” *Int. J. Theor. Phys.* **21**, 467 (1982).
- ²I. M. Georgescu, S. Ashhab, and F. Nori, “Quantum simulation,” *Rev. Mod. Phys.* **86**, 153 (2014).
- ³S. Somaroo, C. H. Tseng, T. F. Havel, R. Laflamme, and D. G. Cory, “Quantum simulations on a quantum computer,” *Phys. Rev. Lett.* **82**, 5381 (1999).
- ⁴J. Clarke and F. K. Wilhelm, “Superconducting quantum bits,” *Nature* **453**, 1031 (2008).
- ⁵J. Q. You and F. Nori, “Atomic physics and quantum optics using superconducting circuits,” *Nature* **474**, 589 (2011).
- ⁶M. H. Devoret and R. J. Schoelkopf, “Superconducting circuits for quantum information: An outlook,” *Science* **339**, 1169 (2013).
- ⁷C. Neill, P. Roushan, K. Kechedzhi, S. Boixo, S. V. Isakov, V. Smelyanskiy, A. Megrant, B. Chiaro, A. Dunsworth, K. Arya, R. Barends, B. Burkett, Y. Chen, Z. Chen, A. Fowler, B. Foxen, M. Giustina, R. Graff, E. Jeffrey, T. Huang, J. Kelly, P. Klimov, E. Lucero, J. Mutus, M. Neeley, C. Quintana, D. Sank, A. Vainsencher, J. Wenner, T. C. White, H. Neven, and J. M. Martinis, “A blueprint for demonstrating quantum supremacy with superconducting qubits,” *Science* **360**, 195 (2018).
- ⁸G. Wendin, “Quantum information processing with superconducting circuits: A review,” *Rep. Prog. Phys.* **80**, 106001 (2017).

- ⁹P. J. J. O'Malley, R. Babbush, I. D. Kivlichan, J. Romero, J. R. McClean, R. Barends, J. Kelly, P. Roushan, A. Tranter, N. Ding, B. Campbell, Y. Chen, Z. Chen, B. Chiaro, A. Dunsworth, A. G. Fowler, E. Jeffrey, E. Lucero, A. Megrant, J. Y. Mutus, M. Neeley, C. Neill, C. Quintana, D. Sank, A. Vainsencher, J. Wenner, T. C. White, P. V. Coveney, P. J. Love, H. Neven, A. Aspuru-Guzik, and J. M. Martinis, "Scalable Quantum Simulation of Molecular Energies," *Phys. Rev. X* **6**, 031007 (2016).
- ¹⁰A. Kandala, A. Mezzacapo, K. Temme, M. Takita, M. Brink, J. M. Chow, and J. M. Gambetta, "Hardware-efficient variational quantum eigensolver for small molecules and quantum magnets," *Nature* **549**, 242 (2017).
- ¹¹A. Y. Kitaev, "Fault-tolerant quantum computation by anyons," *Ann. Phys.* **303**, 2 (2003).
- ¹²N. Goldman, and J. Dalibard, "Periodically Driven Quantum Systems: Effective Hamiltonians and Engineered Gauge Fields," *Phys. Rev. X* **4**, 031027 (2014).
- ¹³P. Roushan, C. Neill, A. Megrant, Y. Chen, R. Babbush, R. Barends, B. Campbell, Z. Chen, B. Chiaro, A. Dunsworth, A. Fowler, E. Jeffrey, J. Kelly, E. Lucero, J. Mutus, P. J. J. O'Malley, M. Neeley, C. Quintana, D. Sank, A. Vainsencher, J. Wenner, T. White, E. Kapit, H. Neven, and J. Martinis, "Chiral ground-state currents of interacting photons in a synthetic magnetic field," *Nat. Phys.* **13**, 146 (2017).
- ¹⁴Y. Wu, L.-P. Yang, M. Gong, Y. Zheng, H. Deng, Z. Yan, Y. Zhao, K. Huang, A. D. Castellano, W. J. Munro, K. Nemoto, D.-N. Zheng, C. P. Sun, Y. xi Liu, X. Zhu, and L. Lu, "An efficient and compact switch for quantum circuits," *npj Quantum Inf.* **4**, 50 (2018).
- ¹⁵X. Li, Y. Ma, J. Han, T. Chen, Y. Xu, W. Cai, H. Wang, Y. Song, Z.-Y. Xue, Z.-q. Yin, and L. Sun, "Perfect quantum state transfer in a superconducting qubit chain with parametrically tunable couplings," *Phys. Rev. Appl.* **10**, 054009 (2018).
- ¹⁶D.-W. Wang, C. Song, W. Feng, H. Cai, D. Xu, H. Deng, H. Li, D. Zheng, X. Zhu, H. Wang, S.-Y. Zhu, and M. O. Scully, "Synthesis of antisymmetric spin exchange interaction and chiral spin clusters in superconducting circuits," *Nat. Phys.* **15**, 382 (2019).
- ¹⁷W. Cai, J. Han, F. Mei, Y. Xu, Y. Ma, X. Li, H. Wang, Y. P. Song, Z.-Y. Xue, Z.-q. Yin, S. Jia, and L. Sun, "Observation of topological magnon insulator states in a superconducting circuit," *Phys. Rev. Lett.* **123**, 080501 (2019).
- ¹⁸O. Kyriienko and A. S. Sørensen, "Floquet quantum simulation with superconducting qubits," *Phys. Rev. Appl.* **9**, 064029 (2018).
- ¹⁹M. Sameti and M. J. Hartmann, "Floquet engineering in superconducting circuits: From arbitrary spin-spin interactions to the Kitaev honeycomb model," *Phys. Rev. A* **99**, 012333 (2019).
- ²⁰X. G. Wen, *Quantum Field Theory of Many-body Systems* (Oxford University Press, New York, 2004).
- ²¹M. Hafezi, P. Adhikari, and J. M. Taylor, "Engineering three-body interaction and Pfaffian states in circuit QED systems," *Phys. Rev. B* **90**, 060503 (2014).
- ²²X. G. Wen, F. Wilczek, and A. Zee, "Chiral spin states and superconductivity," *Phys. Rev. B* **39**, 11413 (1989).
- ²³Y. Taguchi, Y. Oohara, H. Yoshizawa, N. Nagaosa, and Y. Tokura, "Spin chirality, berry phase, and anomalous hall effect in a frustrated ferromagnet," *Science* **291**, 2573 (2001).
- ²⁴D. Grohol, K. Matan, J.-H. Cho, S.-H. Lee, J. W. Lynn, D. G. Nocera, and Y. S. Lee, "Spin chirality on a two-dimensional frustrated lattice," *Nat. Mater.* **4**, 323 (2005).
- ²⁵P. Bruno, V. K. Dugaev, and M. Taillefermier, "Topological hall effect and berry phase in magnetic nanostructures," *Phys. Rev. Lett.* **93**, 096806 (2004).
- ²⁶H. Katsura, N. Nagaosa, and P. A. Lee, "Theory of the thermal hall effect in quantum magnets," *Phys. Rev. Lett.* **104**, 066403 (2010).
- ²⁷M. Hirschberger, R. Chisnell, Y. S. Lee, and N. Ong, "Thermal hall effect of spin excitations in a kagome magnet," *Phys. Rev. Lett.* **115**, 106603 (2015).
- ²⁸Y. Lyanda-Geller, S. H. Chun, M. B. Salamon, P. M. Goldbart, P. D. Han, Y. Tomioka, A. Asamitsu, and Y. Tokura, "Charge transport in manganites: Hopping conduction, the anomalous hall effect, and universal scaling," *Phys. Rev. B* **63**, 184426 (2001).
- ²⁹B. Bauer, L. Cincio, B. Keller, M. Dolfi, G. Vidal, S. Trebst, and A. Ludwig, "Chiral spin liquid and emergent anyons in a kagome lattice mott insulator," *Nat. Commun.* **5**, 5137 (2014).
- ³⁰Y. Zhou, K. Kanoda, and T.-K. Ng, "Quantum spin liquid states," *Rev. Mod. Phys.* **89**, 025003 (2017).
- ³¹M. Christandl, N. Datta, A. Ekert, and A. J. Landahl, "Perfect state transfer in quantum spin networks," *Phys. Rev. Lett.* **92**, 187902 (2004).
- ³²R. Barends, J. Kelly, A. Megrant, D. Sank, E. Jeffrey, Y. Chen, Y. Yin, B. Chiaro, J. Mutus, C. Neill, P. O'Malley, P. Roushan, J. Wenner, T. C. White, A. N. Cleland, and J. M. Martinis, "Coherent josephson qubit suitable for scalable quantum integrated circuits," *Phys. Rev. Lett.* **111**, 080502 (2013).
- ³³C. Song, K. Xu, H. Li, Y.-R. Zhang, X. Zhang, W. Liu, Q. Guo, Z. Wang, W. Ren, J. Hao, H. Feng, H. Fan, D. Zheng, D.-W. Wang, H. Wang, and S.-Y. Zhu, "Generation of multicomponent atomic schrödinger cat states of up to 20 qubits," *Science* **365**, 574 (2019).
- ³⁴D.-W. Wang, H. Cai, R.-B. Liu, and M. O. Scully, "Mesoscopic superposition states generated by synthetic spin-orbit interaction in fock-state lattices," *Phys. Rev. Lett.* **116**, 220502 (2016).
- ³⁵J. K. Pachos and M. B. Plenio, "Three-spin interactions in optical lattices and criticality in cluster hamiltonians," *Phys. Rev. Lett.* **93**, 056402 (2004).
- ³⁶J. K. Pachos and E. Rico, "Effective three-body interactions in triangular optical lattices," *Phys. Rev. A* **70**, 053620 (2004).
- ³⁷D. I. Tsomokos, J. J. García-Ripoll, N. R. Cooper, and J. K. Pachos, "Chiral entanglement in triangular lattice models," *Phys. Rev. A* **77**, 012106 (2008).
- ³⁸Y.-X. Chen, S.-W. Li, and Z. Yin, "Quantum correlations in a clusterlike system," *Phys. Rev. A* **82**, 052320 (2010).

Supplementary Material for “Synthesizing three-body interaction of spin chirality with superconducting qubits”

Wuxin Liu,^{*} Wei Feng,^{*} Wenhui Ren, Da-Wei Wang,[†] and H. Wang[‡]

¹ *Interdisciplinary Center for Quantum Information and Zhejiang Province Key Laboratory of Quantum Technology and Device, Department of Physics, Zhejiang University, Hangzhou 310027, China*

(Dated: February 7, 2020)

I. DEVICE PARAMETERS

Detailed device parameters can be found in Table S1.

TABLE S1. Device parameters. ω_j^{\max} is the maximum frequency of Q_j . ω_j^{idle} is the idle frequency of Q_j , where qubit rotations and state readout are performed. $T_{1,j}$ is the energy relaxation time measured for a qubit under the Floquet modulation with $\omega_0/2\pi \approx 4.990$ GHz and $\Delta/2\pi \approx 138$ MHz, and $T_{2,j}^*$ is the Ramsey Gaussian dephasing time for a qubit biased at around 4.990 GHz. Since in the experiment all three qubits are modulated around ω_0 with microwave excitations being transferred among them, we use a much longer pure dephasing time $\sim 5 \mu\text{s}$, instead of $T_{2,j}^*$, for all qubits in numerical simulation¹. η_j is the qubit anharmonicity. ω_j^r is the resonant frequency of the readout resonator for each qubit. $F_{0,j}$ ($F_{1,j}$) is the typical probability of measuring Q_j in $|0\rangle$ ($|1\rangle$) when Q_j is prepared in $|0\rangle$ ($|1\rangle$), which is used to correct the measured multiqubit probabilities for elimination of the readout errors. The Q_j - Q_k coupling strength g_{jk} is measured by exciting one of the qubits and then bringing both qubits on resonance at ≈ 4.990 GHz while all the other qubits are at their maximum frequencies.

	Q_1	Q_2	Q_3
$\omega_j^{\max}/2\pi$ (GHz)	5.767	6.113	6.062
$\omega_j^{\text{idle}}/2\pi$ (GHz)	5.025	5.380	4.650
$T_{1,j}$ (μs)	18.3	12.3	16.6
$T_{2,j}^*$ (μs)	1.6	0.9	1.1
$\eta_j/2\pi$ (MHz)	-237	-234	-234
$\omega_j^r/2\pi$ (GHz)	6.541	6.659	6.687
F_j^0	0.984	0.932	0.957
F_j^1	0.939	0.906	0.938
	$Q_1 - Q_2$	$Q_1 - Q_3$	$Q_2 - Q_3$
$g_{jk}/2\pi$ (MHz)	12.7	12.4	9.8

II. SINGLE-QUBIT MODULATION

As mentioned in the main text, two qubits can also be dynamically decoupled by modulating only one of them. In this case, the effective coupling strength g_{eff} is $gJ_0(\Delta/\nu)$. We confirm this effect by performing an experiment based on the pulse sequence shown in Fig. S1(a), in which Q_2 is modulated with fixed frequency $\nu/2\pi = 100$ MHz centering at Q_1 's frequency for a period T . The probability of state $|01\rangle$ is measured as a function of T with different modulation amplitudes Δ

and the resulting Rabi oscillations between Q_1 and Q_2 is shown in Fig. S1(b). In Fig. S1(c), $|g_{\text{eff}}|$ as a function of Δ (dots) is obtained by Fourier transform of the experimental data along the time axis in Fig. S1(b). When $\Delta/2\pi \approx 240$ MHz, the effective coupling strength $|g_{\text{eff}}|$ becomes zero and the two qubits are dynamically decoupled, which agrees well with the numerical simulation result (line) in Fig. S1(c).

III. PROCEDURE OF TUNING UP THE THREE-QUBIT CHIRAL DYNAMICS

The procedure to obtain the chiral dynamics (Figs. 3 and 4 of the main text) consists of three steps as sequentially illustrated in Fig. 1, Fig. S1, and Fig. 2.

Step 1: We measure the resonant frequency ω_j versus Z bias curve for each qubit (Fig. 1 of the main text). *Step 2:* For a pair of qubits, we modulate one qubit in frequency centering around the other one which is fixed in frequency (Fig. S1), according to the ω_j versus Z bias curves obtained in step 1. The measurement results can be used to calibrate the drive amplitudes Δ , since the decoupling amplitude is supposed to be 2.404 times the modulation frequency. *Step 3:* With the drive amplitudes being calibrated for the pair of qubits, we then modulate both qubits simultaneously while varying the relative phase of the two modulation drives (Fig. 2 of the main text). The measurement results can be used to calibrate the relative phases since the decoupling point is supposed to be $2\pi/3$.

Using the drive amplitudes and relative phases calibrated above for pairs of qubits, we can assemble the experimental pulse sequences and measure the 3-qubit chiral dynamics data, which clearly demonstrate chiral flows of the qubit excitations as expected. We then fine-tune the drive amplitude, phase, and offset for each qubit around the calibrated values to maximize the oscillation amplitudes, i.e., for the best quality of the data as shown in Figs. 3 and 4 of the main text. In the numerical simulation we also fine-tune the amplitude, phase, and offset of the Floquet modulation around the nominal experimental values for each qubit to obtain a good numerical match with the experimental data.

IV. DERIVATION OF THE EFFECTIVE HAMILTONIAN

When the frequencies of the three qubits are modulated according to $\omega_j(t) = \omega_0 + \Delta \cos(\nu t + 2\pi j/3)$, the Hamiltonian in the interaction picture is

$$\begin{aligned} H_I &= \sum_{jk} \hbar g \sigma_j^+ \sigma_k^- e^{if[\sin(\nu t + 2\pi j/3) - \sin(\nu t + 2\pi k/3)]} + \text{h.c.} \\ &= \sum_{jk} \hbar g \sigma_j^+ \sigma_k^- e^{if2 \sin(\pi/3) \cos[\nu t + \frac{(j+k)\pi}{3}]} + \text{h.c.} \end{aligned} \quad (\text{S1})$$

where $f = \Delta/\nu$. The above Hamiltonian can be expanded to $H_I = \sum_n H_n e^{in\nu t}$ with

$$H_0 = \hbar g J_0 (\sqrt{3}f) \sum_{jk} \sigma_j^+ \sigma_k^- + \text{h.c.}, \quad (\text{S2})$$

$$H_n = \hbar g i^n J_n (\sqrt{3}f) e^{\frac{in(j+k)\pi}{3}} \sum_{jk} [\sigma_j^+ \sigma_k^- + (-1)^n \sigma_j^- \sigma_k^+]. \quad (\text{S3})$$

Under the condition $\nu \gg g$, we obtain the effective Floquet Hamiltonian²

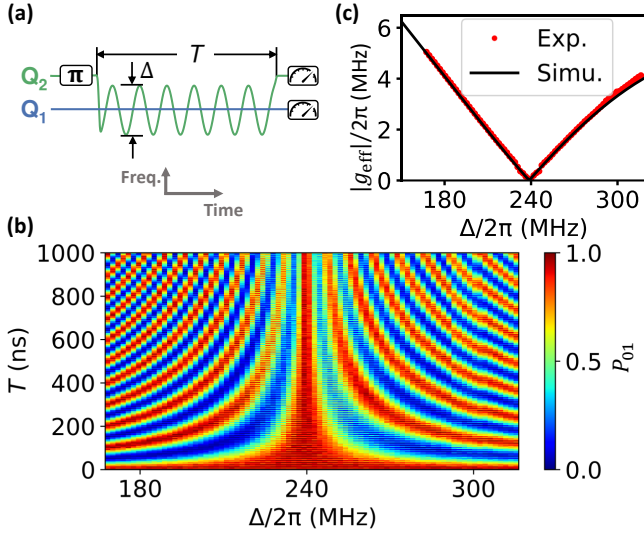


FIG. S1. (a) Pulse sequence with the single-qubit modulation to tune the effective coupling strength g_{eff} between Q_1 and Q_2 . Both qubits are initialized in $|0\rangle$ while all the other qubits on the same chip are far detuned. Then Q_2 is excited to $|1\rangle$ by a π rotation and after that its frequency is sinusoidally modulated for a period T , during which Q_1 's frequency is fixed at ≈ 4.990 GHz. The center of the sinusoidal modulation is fixed at Q_1 's frequency and the modulation frequency $\nu/2\pi = 100$ MHz is also fixed while the modulation amplitude Δ is varied. Finally the probability of the Q_1 - Q_2 joint state $|01\rangle$, P_{01} , is measured. (b) P_{01} measured as a function of T and Δ . (c) Effective coupling strength $|g_{\text{eff}}|$ as a function of Δ (dots), obtained by Fourier transform of the data in (b), in comparison with the numerical simulation result (line).

$$H_{\text{eff}} \approx H_0 + \sum_{n=1}^{\infty} \frac{1}{n\hbar\nu} [H_n, H_{-n}], \quad (\text{S4})$$

where

$$[H_n, H_{-n}] = \sum_{jkl} \hbar^2 g^2 J_n^2 (\sqrt{3}f) \sin\left(\frac{n\pi}{3}\right) \sigma_j^z (\sigma_k^x \sigma_l^y - \sigma_k^y \sigma_l^x). \quad (\text{S5})$$

By setting $J_0(\sqrt{3}f) = 0$ with $\Delta/\nu = 2.404/\sqrt{3}$, we obtain $H_0 = 0$, and

$$H_{\text{eff}} = \hbar \kappa \hat{\chi}, \quad (\text{S6})$$

where $\kappa = g^2 \beta / \nu$ and $\beta = \sum_{n=1}^{\infty} J_n^2(\sqrt{3}f) \sin(n\pi/3)/n$.

V. EFFECT OF WEAK ANHARMONICITY

The transmon qubit is not a pure two-level system, which has multiple energy levels and the energy separations between adjacent two levels are not equal. Qubit anharmonicity is defined by $\eta = \omega^{21} - \omega^{10}$, where ω^{lm} is the transition frequency between levels l and m ($l, m = 0, 1, 2, \dots$, and the ground state corresponds to level 0). Here we consider the effect of η by including three energy levels, $\{|0\rangle, |1\rangle, |2\rangle\}$, for each transmon qubit. Note that when the sinusoidal modulation pulse is applied to the transmon qubit, both ω^{21} and ω^{10} vary simultaneously over time and η remains almost a constant. The full Hamiltonian is

$$\begin{aligned} H &= \hbar \sum_{j=1}^3 \left[\omega_j^{10}(t) |1\rangle_j \langle 1|_j + [2\omega_j^{10}(t) + \eta_j] |2\rangle_j \langle 2|_j \right] \\ &+ \hbar g \sum_{jk} \left(|1\rangle_j \langle 0|_j |0\rangle_k \langle 1|_k + \text{h.c.} \right) \\ &+ \sqrt{2} \hbar g \sum_{jk} \left(|2\rangle_j \langle 1|_j |0\rangle_k \langle 1|_k + \text{h.c.} \right) \\ &+ 2\hbar g \sum_{jk} \left(|2\rangle_j \langle 1|_j |1\rangle_k \langle 2|_k + \text{h.c.} \right), \end{aligned} \quad (\text{S7})$$

which is used in numerical simulation.

When there is no population in $|2\rangle$ of any of the three qubits during the qubit initialization stage, the total effective Hamiltonian of the system under the Floquet modulation pulses can be restricted to the subspace $\{|0\rangle, |1\rangle\}$ for each qubit, and under the assumption $|n\nu + \eta| \gg gJ_n(\sqrt{3}f)$ we have

$$H_{\text{eff}} \approx H_0 + \hbar \kappa \hat{\chi} + \left[\hbar \kappa' (S_z + 1/2) \sum_{jk} \sigma_j^+ \sigma_k^- + \text{h.c.} \right], \quad (\text{S8})$$

where $S_z = \sum_j \sigma_j^z / 2$, $\kappa' = -2g^2 \sum_{n=-\infty}^{+\infty} \frac{J_n^2(\sqrt{3}f)}{n\nu+\eta} e^{in\pi/3}$ is an additional second-order coupling between qubits due to the existence of $|2\rangle$. We note that, for $n = 2$, $|n\nu+\eta| \approx 6gJ_n(\sqrt{3}f)$ in our experiment and the assumption may not be well satisfied. However, our numerical simulation results are based on the full Hamiltonian of Eq. (1) in the main text without any approximation, and the apparent agreement with the experimental data indicates that our theory still works decently.

In general, κ' is a complex number and it can be rewritten as $\kappa' = \alpha + i\lambda$. With $\hat{E}_s = \sum_{jk} (\sigma_j^+ \sigma_k^- + \sigma_j^- \sigma_k^+)$ being the symmetric exchange interaction and $\hat{E}_{as} = i \sum_{jk} (\sigma_j^+ \sigma_k^- - \sigma_j^- \sigma_k^+)$ being the antisymmetric exchange interaction, the effective Hamiltonian can be written as (note that $\hat{E}_{as} = S_z \hat{\chi}$)

$$\begin{aligned} H_{\text{eff}} &= H_0 + \hbar\kappa\hat{\chi} + \frac{1}{2}\hbar\lambda \left(S_z \hat{\chi} + \frac{1}{2}\hat{\chi} \right) + \hbar\alpha (S_z + 1/2) \hat{E}_s \\ &= H_0 + \hbar \left[\left(\kappa + \frac{\lambda}{4} \right) + \frac{\lambda}{2} S_z \right] \hat{\chi} + \hbar\alpha (S_z + 1/2) \hat{E}_s. \end{aligned} \quad (\text{S9})$$

Using the experimental parameters, $\nu = 100$ MHz, $\Delta =$

138 MHz, and $\eta = -234$ MHz, we have $J_0(\sqrt{3}f) \approx 0$, $\alpha \approx 0$, and

$$H_{\text{eff}} \approx \hbar \left[\left(\kappa + \frac{\lambda}{4} \right) + \frac{\lambda}{2} S_z \right] \hat{\chi}. \quad (\text{S10})$$

Here α is actually slightly negative. Since H_0 contains the \hat{E}_s term with the coefficient $gJ_0(\sqrt{3}f)$, to cancel this negative α we can reduce the modulation amplitudes so that $gJ_0(\sqrt{3}f)$ becomes slightly positive, as experimentally observed. In the numerical simulation results in Fig. 4 of the main text, we choose $\Delta_j/2\pi = \{135 \text{ MHz}, 137 \text{ MHz}, 133 \text{ MHz}\}$ for $Q_j = \{Q_1, Q_2, Q_3\}$ while all other parameters remain the same as those used in the numerical simulation of Fig. 3, and a good agreement between the numerical results and the experimental data is obtained.

In the case of a single excitation, $S_z = -1/2$ and the coupling strength is κ . However, the coupling strength is $\kappa + \lambda/2$ with $S_z = 1/2$ when there are two excitations. Therefore, the circulation for the two-excitation case is faster than that for the single-excitation case with $\lambda > 0$, as experimentally observed in Figs. 3 and 4 of the main text.

* W. L. and W. F. contributed equally to this work.

† dwwang@zju.edu.cn

‡ hhwang@zju.edu.cn

¹ K. Xu, J.-J. Chen, Y. Zeng, Y.-R. Zhang, C. Song, W. Liu, Q. Guo, P. Zhang, D. Xu, H. Deng, K. Huang, H. Wang, X. Zhu, D. Zheng, and H. Fan, "Emulating many-body local-

ization with a superconducting quantum processor," *Phys. Rev. Lett.* **120**, 050507 (2018).

² N. Goldman and J. Dalibard, "Periodically Driven Quantum Systems: Effective Hamiltonians and Engineered Gauge Fields," *Phys. Rev. X* **4**, 031027 (2014).